Efficient BI-RME Method Implementation for the Full-Wave Analysis of Passive Devices based on Circular Waveguides with Arbitrary Perturbations

Carlos Carceller[1], Santiago Cogollos[1], Pablo Soto[1], Jordi Gil[2], Vicente E. Boria[1], Carlos Vicente[2] and Benito Gimeno[3]

[1]Departamento de Comunicaciones, Instituto de Telecomunicaciones y Aplicaciones Multimedia, Universidad Politécnica de Valencia, E-46022, Valencia, Spain (*carcarc2@upvnet.upv.es, sancobo@dcom.upv.es, pabsopac@dcom.upv.es, vboria@dcom.upv.es*).
[2]Aurora Software and Testing S.L., E-46022, Valencia, Spain (*jordi.gil@aurorasat.es, carlos.vicente@aurorasat.es*).
[3]Departamento de Física Aplicada, Instituto de Ciencia de Materiales, Universidad de Valencia, E-46100, Burjassot, Spain (*benito.gimeno@uv.es*).

Abstract

In this paper, the efficient full-wave analysis of passive devices composed of circular and arbitrarily-shaped waveguides is considered. For this purpose, the well-known Boundary Integral - Resonant Mode Expansion (BI-RME) method has been properly extended. Circular waveguides are used for the resonant mode expansion, whereas the arbitrary contour is defined by any combination of straight, circular and elliptical segments, thus allowing the exact representation of the most widely used geometries. The proposed algorithm extends previous implementations of the BI-RME method based on circular waveguides by considering circular and elliptical arcs for defining arbitrary geometries. Likewise, it allows the efficient analysis of passive devices based on circular waveguides with arbitrary perturbations, thus providing more accurate results with less computational efforts than a rectangular waveguide based BI-RME approach. The extended method has been successfully tested with several practical application examples, having compared its performance with the BI-RME method based on rectangular waveguides.

I. Introduction

Nowadays, many waveguide components for satellite applications are based on cylindrical cavities. Examples of such components include dual-mode filters, polarisers, sidewall-coupled cylindrical cavity filters, etc. (see [1]). The high electrical response sensitivity found in some of these components, e.g. dual-mode filters, has encouraged the development of full-wave electromagnetic analysis tools for its accurate and efficient modeling.

The analysis of complex waveguide components has been traditionally carried out by means of segmenting the structure into simpler building blocks: waveguide sections, discontinuities and planar junctions, as described in [2]. Instead of considering the structure as a whole, it is simpler and computationally more efficient to analyse different types of blocks independently, and eventually combine them to obtain the component response. In order to

characterize any waveguide section, it is essential to compute its modal chart. For the full-wave characterization of planar junctions and discontinuities, the modal coupling coefficients of the involved waveguides are also required. Consequently, full-wave modal analysis methods are generally focused on computing these two sets of parameters.

Over the last decades, a wide number of analysis techniques have been reported in the technical literature. On the one hand, there are techniques based on the solution of an integral equation by the method of moments (MoM) [3]-[4] which solve a non-linear eigenvalue problem of small size. On the other hand, there are techniques based on discretization methods leading to large algebraic problems, such as Finite-Element (FE) [5] or Finite Difference Time Domain (FD-TD) methods [6]. Recently, hybrid techniques have been proposed in order to mitigate the drawbacks of both groups. Some methods that fall into this category are the mode-matching finite-element (MM/FE) method [7], the boundary contour mode-matching (BCMM) method [8], and the combination of the mode-matching, finite-element, method of moments and finite difference methods (MM/FE/MoM/FD) [9].

In this paper, a technique which combines the flexibility of discretization methods with the efficiency of modal techniques is extended, the so called 2D Boundary Integral - Resonant Mode Expansion (BI-RME) method [10]. The first original publication of this technique [11] considered its application to the modal analysis of arbitrary-contour waveguide structures by means of the combination of an integral equation with the modal expansion of a two-dimensional resonant contour. After solving a linear matrix eigenvalue problem, the BI-RME method provides the modal chart of the arbitrarily shaped waveguide structure. The linear character of the matrix problem offers a great advantage over methods that solve integral equations through frequency-dependent eigenvalue problems, which typically result in larger computational efforts. Moreover, the moderate size of the matrices involved in the BI-RME method, reduces the amount of required memory resources, specially when compared with discretization techniques. Furthermore, the use of the BI-RME method within optimization procedures offers great advantages since, from one iteration to the next one of these processes, only the integrals that involve altered geometries need to be recomputed.

After the first publication of the BI-RME method, the technique was revisited to additionally provide the coupling coefficients between the arbitrarily shaped waveguide and the basic resonant contour [12]. For this purpose, the same matrices involved in the solution of the eigenvalue problem were used, thus adding very little computational effort. Further efforts were done in the direction of extending the original method in order to include circular and elliptical arcs to describe the arbitrarily-shaped structure, since the original work [11] only considered straight segments. In [13], these two kinds of segments were added for the BI-RME method formulated in terms of rectangular waveguide modes. For such case, it was proved that the accuracy can be increased, specially when computing the cut-off frequencies of the lower order modes of such arbitrary waveguides.

However, that work has proven to be inefficient for the analysis of devices based on circular waveguides. In such

cases the rectangular-based implementation of the BI-RME method requires a large number of resonant modes to compute the modal chart of the arbitrary waveguide with a high degree of accuracy. Likewise, the arbitrary waveguides that typically compose these devices are usually connected to other circular waveguides. Therefore the rectangular-based implementation does not take advantage of the efficient computation of coupling coefficients provided by the BI-RME method [12]. These drawbacks can be avoided with the new BI-RME implementation presented in this paper, which combines the use of a circular waveguide as the resonant contour with the possibility of using circular and elliptical arcs (together with straight segments) for defining the arbitrary geometry. With this implementation based on circular waveguides, many practical passive devices can be analysed and designed more accurately and with less CPU time than using the rectangular-based algorithm.

II. THEORY

The basic structure under analysis (see Fig. 1) is an arbitrarily-shaped waveguide whose cross section Ω is defined by the contour σ. In order to analyse this waveguide, it will be enclosed within a standard circular waveguide S_0 and the original BI-RME formulation [11] will be applied.

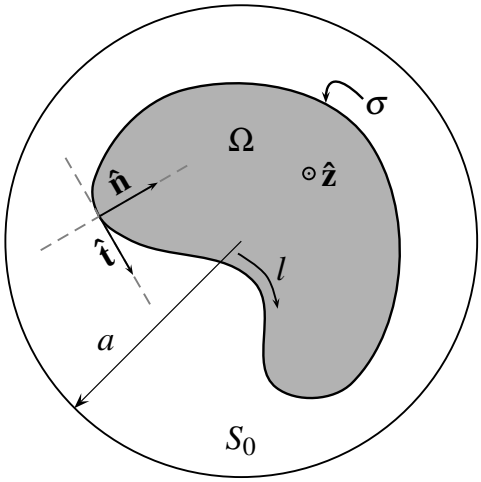

Fig. 1. Basic contour of the arbitrary waveguide enclosed within a basic circular contour.

A. Computation of the TM Modes

To compute the TM modes of an arbitrarily shaped waveguide by means of the BI-RME method, it is necessary to compute two matrices, $\mathbf{L}'$ and $\mathbf{R}'$ [11]. The matrix $\mathbf{R}'$ is related to the resonant-mode expansion of the basic circular waveguide. The matrix $\mathbf{L}'$ involves the scalar Green's function g for the cylindrical resonator. This paper only deals with the $\mathbf{L}'$ matrix, since the computation of the $\mathbf{R}'$ matrix can be easily performed using standard numerical integration methods. The elements of $\mathbf{L}'$ can be expressed as follows

$$L'_{ij} = \int_\sigma \int_\sigma w_i(l)\ g(\mathbf{s}, \mathbf{s}')\ w_j(l')\ dl\ dl' \tag{1}$$

where w_i, w_j are the basis and testing functions related to the implementation of the Method of Moments. These functions are piece-wise parabolic splines defined in two or three segments of the arbitrary contour σ. In our proposed enhanced algorithm, these segments can be straight, circular or elliptical arcs, and the basis functions are expressed in terms of a suitable variable l defined on σ as follows:

$$w(l) = al^2 + bl + c \tag{2}$$

Furthermore, $\mathbf{s}$ and $\mathbf{s}'$ represent field and source vectors in the arbitrary contour σ, and g represents the scalar Green's function for two-dimensional resonators of circular cross section. Since g is singular when $\mathbf{s} = \mathbf{s}'$, the diagonal components of $\mathbf{L}'$ manifest a singular behaviour; in these cases the singularity has to be extracted from the computation of the matrix and solved analytically. The non-diagonal components can be easily computed using standard numerical integration techniques (e.g. the Gauss quadrature). According to [11], the expression of the scalar Green's function g for this structure is

$$g(r, \phi, r', \phi') = \frac{1}{2\pi} \ln\left(r' R_i / aR\right) \tag{3}$$

where

$$R = \left(r^2 + r'^2 - 2rr'C\right)^{1/2} \tag{4}$$

$$R_i = \left(r^2 + a^4/r'^2 - 2ra^2C/r'\right)^{1/2} \tag{5}$$

$$C = \cos(\phi - \phi') \tag{6}$$

and a is the radius of the bounding circular contour.

It can be easily observed that the singular behaviour of g is of the type $\ln(R)$ when the field point $\mathbf{s}(r, \phi)$ approaches the source point $\mathbf{s}'(r', \phi')$, since R represents the distance between these two sets of points. To isolate the problematic behaviour of this term, it is necessary to split the Green's function into a regular and a singular term, dealing with each of them separately

$$g = g^{reg} + g^{sing} = \frac{1}{4\pi} \ln\left(\frac{r' R_i}{a}\right)^2 - \frac{1}{4\pi} \ln\left(R^2\right) \tag{7}$$

where g^{reg} is regular since

$$\lim_{r\to r'} \ln\left(\frac{r' R_i}{a}\right)^2 = \ln\left[\frac{\left(r'^2 - a^2\right)^2}{a^2}\right] \tag{8}$$

Following this division of g into a regular and a singular part, the double integral of (1) can be split accordingly. On the one hand, the double integral involving g^{reg} can be solved numerically, as it is done with the rest of the integrals that do not present a singular behaviour (such as the elements of matrix $\mathbf{R}'$). On the other hand, the double integral involving g^{sing} can be performed in two steps. Firstly, the line integral with respect to the primed coordinates is solved analytically, due to its singular behaviour. For circular and elliptical arcs, this singular integral can be computed analytically using a procedure totally equivalent to the one described in [13]. Then, the line integral with respect to the non-primed coordinates is computed numerically, since it has now a regular form.

B. Computation of the TE Modes

The accurate computation of TE modes depends on the capability to evaluate the matrices $\mathbf{C}$ and $\mathbf{L}$, whose elements are

$$C_{ij} = \int_\sigma \int_\sigma g(\mathbf{s}, \mathbf{s}') \frac{\partial w_i(l)}{\partial l} \frac{\partial w_j(l')}{\partial l'}\, dl\, dl' \tag{9}$$

$$L_{ij} = \int_\sigma \int_\sigma w_i(l) w_j(l')\ \hat{\mathbf{t}}(l) \cdot \overline{\mathbf{G}}_{st}\left(\mathbf{s}, \mathbf{s}'\right)\ \cdot \hat{\mathbf{t}}(l')\, dl\, dl' \tag{10}$$

where $w_n(l)$ and $\partial w_n(l)/\partial l$ are, respectively, the basis functions and their derivatives, $\hat{\mathbf{t}} = t_r \hat{\mathbf{r}} + t_\phi \hat{\boldsymbol{\phi}}$ is the vector tangent to the contour σ, and $\overline{\mathbf{G}}_{st}$ is the solenoidal dyadic Green's function.

As it can be observed, equation (9) is very similar to (1), with the only difference being the presence of the derivatives instead of the basis functions. Therefore, the procedure to solve the singularity inherent to the scalar Green's function in the $\mathbf{C}$ matrix is completely equivalent to the one previously described for the $\mathbf{L}'$ matrix of TM modes, with the consideration that the derivatives of the basis functions are linear splines (i.e. $a = 0$ in (2)).

The computation of the $\mathbf{L}$ matrix requires to manage the solenoidal dyadic Green's function, which can be expressed as follows [11]

$$\begin{aligned} \overline{\mathbf{G}}_{st}\left(r, \phi, r', \phi'\right) &= G_{rr}\ \hat{\mathbf{r}}\hat{\mathbf{r}}' + G_{\phi r}\ \hat{\boldsymbol{\phi}}\hat{\mathbf{r}}' \\ &+ G_{r\phi}\ \hat{\mathbf{r}}\hat{\boldsymbol{\phi}}' + G_{\phi\phi}\ \hat{\boldsymbol{\phi}}\hat{\boldsymbol{\phi}}' \end{aligned} \tag{11}$$

being

$$G_{rr} = \frac{1}{8\pi}\left[2C\,\ln\left(\frac{r' R_i}{a\,R}\right) + \frac{\left(r^2 + r'^2\right) C - 2rr'}{R^2} + \frac{\left(r^2 + r'^2 + 4a^2\right) C - 2rr'}{\left(r' R_i / a\right)^2} - \left(1 + \frac{a^2}{r^2}\right)\left(1 + \frac{a^2}{r'^2}\right) \cdot \cdot \left(LC - AS + \frac{rr'}{\left(r' R_i / a\right)^2}\right)\right] \tag{12a}$$

$$G_{\phi r} = \frac{1}{8\pi}\left[-2S\,\ln\left(\frac{r' R_i}{a\,R}\right) + \frac{\left(r^2 - r'^2\right) S}{R^2} + \frac{\left(r^2 + r'^2 - 2a^2\right) S}{\left(r' R_i / a\right)^2} + \left(1 - \frac{a^2}{r^2}\right)\left(1 + \frac{a^2}{r'^2}\right)(LS + AC)\right] \tag{12b}$$

$$G_{r\phi} = \frac{1}{8\pi}\left[2S\,\ln\left(\frac{r' R_i}{a\,R}\right) + \frac{\left(r^2 - r'^2\right) S}{R^2} - \frac{\left(r^2 + r'^2 - 2a^2\right) S}{\left(r' R_i / a\right)^2} - \left(1 + \frac{a^2}{r^2}\right)\left(1 - \frac{a^2}{r'^2}\right)(LS + AC)\right] \tag{12c}$$

$$G_{\phi\phi} = \frac{1}{8\pi}\left[2C\,\ln\left(\frac{r' R_i}{a\,R}\right) - \frac{\left(r^2 + r'^2\right) C - 2rr'}{R^2} + \frac{\left(r^2 + r'^2 - 2a^2\right)\left(rr'/a^2 - C\right)}{\left(r' R_i / a\right)^2} - \frac{rr'}{a^2} - \left(1 - \frac{a^2}{r^2}\right)\left(1 - \frac{a^2}{r'^2}\right) \cdot \cdot \left(LC - AS + \frac{rr'}{a^2}\right)\right] \tag{12d}$$

where R, R_i, C are defined in (4)-(6) and

$$L = \ln\left(\frac{r'R_i}{a^2}\right) \tag{13}$$

$$A = \arctan\left(\frac{rr'S}{a^2 - rr'C}\right) \tag{14}$$

$$S = \sin(\phi - \phi') \tag{15}$$

This dyadic Green's function has a singular behaviour due to the term $\ln(r'R_i/a\,R)$ present in the four components. Following a similar procedure to the one used with the TM modes, $\overline{\mathbf{G}}_{st}$ can be split into a regular part and a singular part, being the latter as shown next

$$\begin{aligned}\overline{\mathbf{G}}_{st}^{sing} &= \frac{1}{8\pi}\Big[C\ln(R^2)\,\hat{\mathbf{r}}\hat{\mathbf{r}}' - S\ln(R^2)\,\hat{\boldsymbol{\phi}}\hat{\mathbf{r}}' \\ &+ S\ln(R^2)\,\hat{\mathbf{r}}\hat{\boldsymbol{\phi}}' + C\ln(R^2)\,\hat{\boldsymbol{\phi}}\hat{\boldsymbol{\phi}}'\Big]\end{aligned} \tag{16}$$

As it has been done for the TM modes, the double integral of (10) will be split into an inner line integral that will be solved analytically, due to its singularities, and an outer line integral that will be solved numerically. The singular integral to be solved analytically is

$$L_{sing} = \int_{\sigma} w_j(l')\,\hat{\mathbf{t}}\cdot\overline{\mathbf{G}}_{st}^{sing}\cdot\hat{\mathbf{t}}'dl' \tag{17}$$

where

$$\begin{aligned}\hat{\mathbf{t}}\cdot\overline{\mathbf{G}}_{st}^{sing}\cdot\hat{\mathbf{t}}' &= \frac{\ln R^2}{8\pi}\left[C\left(t_r t_{r'} + t_\phi t_{\phi'}\right)\right. \\ &+ \left. S\left(-t_\phi t_{r'} + t_r t_{\phi'}\right)\right]\end{aligned} \tag{18}$$

Given that

$$t_r\,t_{r'} + t_\phi\,t_{\phi'} = C\left(t_x\,t_{x'} + t_y\,t_{y'}\right) + S\left(t_y\,t_{x'} - t_x\,t_{y'}\right) \tag{19}$$

$$-t_\phi\,t_{r'} + t_r\,t_{\phi'} = S\left(t_x\,t_{x'} + t_y\,t_{y'}\right) - C\left(t_y\,t_{x'} - t_x\,t_{y'}\right) \tag{20}$$

it is immediate to rewrite the singular integral (17) as

$$L_{sing} = \int_{\sigma} w_j(l') \, \frac{\ln R^2}{8\pi} \left(\hat{\mathbf{t}} \cdot \hat{\mathbf{t}}' \right) dl' \tag{21}$$

If the contour σ includes circular and/or elliptical arcs, the analytical computation of this singular integral can be carried out using the technique explained in [13] for TE modes.

III. Numerical Results

In this section, the proposed implementation of the BI-RME method using a circular resonant contour is validated with results from measurements and the technical literature. The first examples show the improvements related to the proposed BI-RME implementation with regard to previous works, due to the introduction of new segments (i.e. circular and elliptical ones), as well as due to the proper election of the resonant contour for the analysis of circular-based devices. An elliptical waveguide has been first considered to illustrate how the introduction of the new arcs increases the efficiency of the method. Likewise, the analysis of a triple-ridge waveguide and a cross-shaped iris have been performed in order to demonstrate how the proper election of the resonant contour can also affect significantly the performance of the algorithm. After integrating the proposed algorithm within a full-wave analysis tool [14], the analysis and design of several complex devices in circular waveguide technology have been carried out. Using this software, a circular waveguide polariser and a dual-mode filter with elliptical irises and tuning elements have been analysed. Additionally, a dual-mode filter with cross-shaped irises and tuning elements has been successfully designed. From this last design a prototype has been manufactured, providing a first-hand set of data to test both the band-of-interest as well as the out-of-band simulated responses.

The results obtained with the circular-based implementation have proven to be highly accurate when compared with available numerical or experimental data. This implementation has also shown a more efficient performance than the rectangular-based implementation for the analysis of all the structures considered in this section. All the CPU times in this section have been obtained using a standard PC with a 2.83 GHz Intel Core 2 Quad processor.

A. Elliptical Waveguide

The first example considers the analysis of an elliptical waveguide (major semi-axis $a = 10$ mm and eccentricity $e = 0.5$). This example highlights the improvement, in terms of accuracy and speed, derived from the inclusion of elliptical arcs to describe arbitrary contours in the presented BI-RME implementation, as opposed to previous implementations that required discretizing the contour with only linear segments.

The contour has been described with both elliptical arcs and straight segments and the circular-based BI-RME algorithm (resonant contour radius $R = 11$ mm) has been applied. The relative errors in the computation of the cut-off wavelength of several modes for each discretization are shown in Table I, along with the CPU times. In

TABLE I

RELATIVE ERROR IN THE CUT-OFF WAVELENGTH COMPUTATION OF THE MODES OF AN ELLIPTICAL WAVEGUIDE ($a = 10$ mm AND $e = 0.5$) DESCRIBING THE STRUCTURE WITH ELLIPTICAL ARCS (4 ARCS) AND LINEAR SEGMENTS (8, 16, 32 AND 80 SEGMENTS). THE REFERENCE WAVELENGTH VALUES USED TO COMPUTE THE RELATIVE ERROR ARE TAKEN FROM [15].

	Cut-off Wavelength Relative Error (%)				
	Elliptical Arcs	Linear Segments			
Mode	4	8	16	32	80
1	0.004	4.886	1.262	0.322	0.055
5	0.021	4.660	1.258	0.337	0.072
10	0.033	4.551	1.251	0.347	0.084
50	0.110	5.991	1.472	0.438	0.161
100	0.401	5.860	1.735	0.692	0.447
Time (s)	0.9	0.9	1.3	2.4	13.5

order to compute this relative error, the cut-off wavelengths computed in [15] using the classical calculation of the parametric zeros of the modified Mathieu functions have been used as a reference.

Additionally, the coupling coefficients between certain modes of the elliptical waveguide and others of the circular contour have been computed for all the examples. The relative error in the computation of these coupling coefficients has been graphically shown in Fig. 2, where the reference values have been taken as those provided by the analysis with elliptical arcs.

From the results included in Table I and Fig. 2, it is obvious that as the number of straight segments used to describe the contour increases, so does the accuracy of the analysis but at the cost of increasing the simulation time. However, the use of elliptical arcs provides the accuracy of a very fine linear-discretization analysis, but with the speed of a coarse discretization one. Achieving high levels of accuracy in a fraction of the time is specially important when optimizing sensitive devices, since the errors in the computation of both the cut-off wavelengths and the coupling coefficients have a huge impact in the overall response of the device and can lead to longer optimization cycles.

B. Multi-ridged Circular Waveguide

Next, the modal chart of a multi-ridge circular waveguide (Fig. 3a) is presented. This structure is especially suitable to be analysed by the circular-based implementation. Thus, it serves the purpose of showing how the proper election of the resonant contour has an impact on the accuracy of the algorithm. This example consists of a circular waveguide of radius $b = 20$ mm with three equidistant metal insertions of angular thickness $t = 20°$. Sweeping the inner radius from $a = 1$ mm to 19 mm, a series of simulations have been performed using the

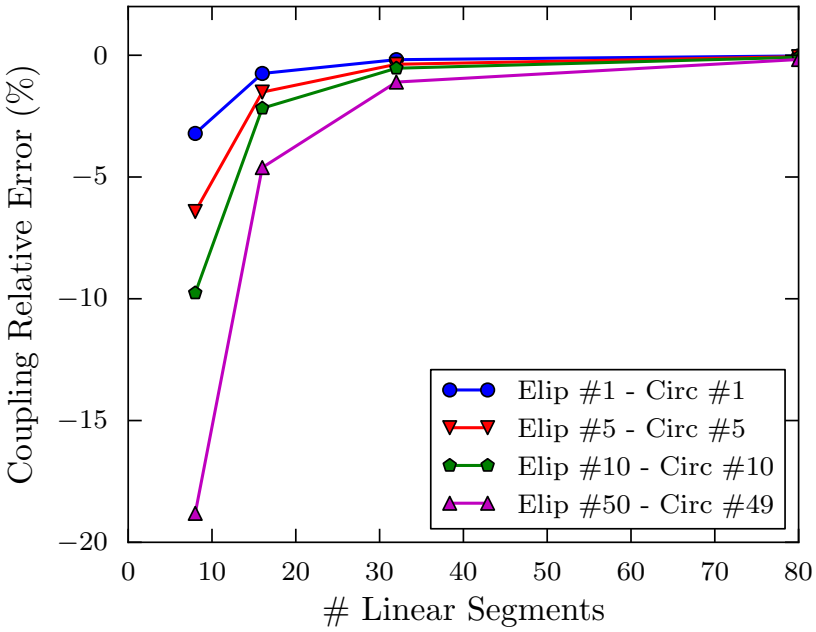

Fig. 2. Relative error in the computation of the coupling coefficients between four pairs of elliptical and circular waveguide modes for different number of linear segments to describe the elliptical contour. The reference values for the computation of the error have been taken as the coupling coefficients provided by the analysis with elliptical arcs.

circular-based implementation ($R = 20$ mm) and the rectangular-based approach ($l = 41$ mm). The results of these simulations can be seen in Fig. 3b, where the cut-off frequencies for the first two TE modes and the first TM mode have been computed and successfully compared with [16] and the measurements of [17]. For low order modes, as the ones considered in Fig. 3b, both the circular and the rectangular-based implementations achieve rapidly convergent results. For instance, only 100 resonant modes have been used with both implementations, requiring less than 0.65 s per simulation point with the rectangular-based code and 0.45 s with the circular-based one.

However, typical analysis of complex passive devices require the use of higher order modes (usually up to 100 modes) for a proper characterization of the structure. In those cases, the performance of the circular-based implementation excels that of the rectangular-based approach, since the structure is based on a circular waveguide. To show this, we have analysed the multi-ridge waveguide setting the inner radius to $a = 16$ mm and studied the convergence of both implementations through the computation of the 100-th mode cut-off frequency. The results of this study are summarized in Table II, where the superior performance of the circular-based implementation over the rectangular one can be observed. In approximately 0.8 s the circular-based algorithm computes the cut-off frequency of this mode with a relative error smaller than 0.1%, while the rectangular-based takes 5.9 s to achieve a similar level of accuracy. The main reason for this important improvement is that the number of segmented portions (red portions in Fig. 3a) is smaller since the majority of the segments are coincident with the outer circular contour, and do no need to be segmented by the circular-based implementation. With a smaller number of portions the size

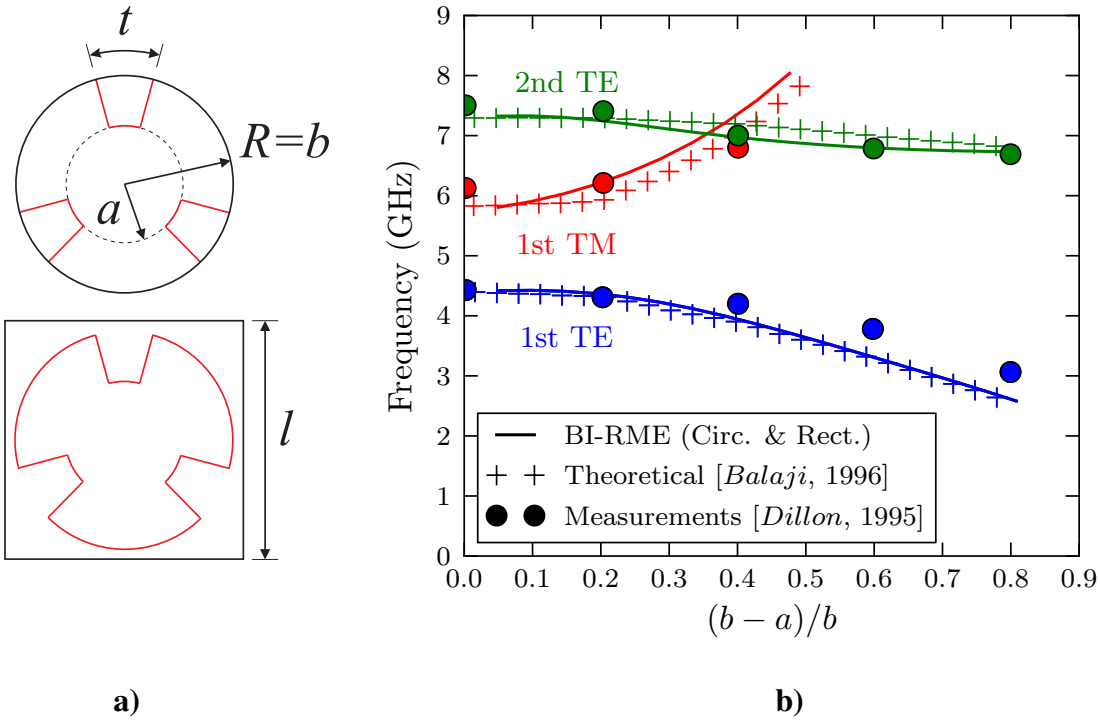

Fig. 3. **a)**: Dimensions of the multi-ridged circular waveguide as well as the circular and square contours used by the BI-RME method. Red lines indicate those segments that have to be considered for the application of the BI-RME method in each case. **b)**: Cut-off frequency for the first two TE modes and the first TM mode of the multi-ridge circular waveguide for different insertion depths (a). Simulations are compared with [16] and measurements of [17].

of the eigenvalue problem decreases, so the time devoted to its construction and solution is drastically reduced.

C. Cross-shaped Iris

In the previous example, it has been demonstrated how the election of the resonant contour has an effect on the accuracy and efficiency of the modal chart calculation. Now, it is shown how this election also affects the computation of coupling coefficients, another key factor when analysing the electromagnetic response of complex devices. For such study, a structure consisting on a cross-shaped iris connected to a circular waveguide is considered, as seen in Fig. 4a. On the one hand, this structure has been analysed with the circular-based algorithm, using the connected circular waveguide (radius $R = 12$ mm) as the resonant contour. This analysis has automatically provided the desired coupling integrals. On the other hand, the structure has been analysed using the rectangular-based algorithm, which computes the coupling coefficients as follows:

$$I_{\bigcirc}^{\triangle} = \sum_{n=1}^{N_r} < \mathbf{e}_i^{\bigcirc}, \mathbf{e}_n^{\square} >< \mathbf{e}_j^{\triangle}, \mathbf{e}_n^{\square} > \tag{22}$$

where $\mathbf{e}_i^{\bigcirc}$ are the modal vectors of the circular waveguide connected to the iris, $\mathbf{e}_i^{\square}$ are the modal vectors of the rectangular box and $\mathbf{e}_j^{\triangle}$ are the modal vectors of the cross-shaped iris. Note that the first inner product in (22) is

TABLE II

CUT-OFF FREQUENCY OF THE 100TH MODE OF THE TRIPLE-RIDGED CIRCULAR WAVEGUIDE ($b = 20$ mm, $a = 16$ mm, $t = 20^\circ$) COMPUTED WITH THE CIRCULAR AND RECTANGULAR-BASED IMPLEMENTATIONS FOR DIFFERENT NUMBER OF RESONANT MODES. THE EXACT CUT-OFF FREQUENCY FOR THE COMPUTATION OF THE RELATIVE ERROR IS TAKEN AS $f_c = 34.8788$ GHz. THE CPU TIME REQUIRED FOR EACH ANALYSIS IS INCLUDED.

# Resonant	Circular-based			Rectangular-based		
Modes	f_c [GHz]	Error (%)	Time (s)	f_c [GHz]	Error (%)	Time (s)
300	34.9050	0.075	0.8	35.0293	0.431	2.2
400	34.8913	0.036	0.9	34.9630	0.241	2.9
500	34.8873	0.024	1.2	34.9363	0.165	3.2
600	34.8861	0.021	1.5	34.9186	0.114	4
700	34.8848	0.017	2	34.9096	0.088	4.9
800	34.8839	0.015	2.3	34.9043	0.073	5.9
900	34.8823	0.010	2.7	34.9003	0.062	6.6
1000	34.8815	0.008	3.2	34.8971	0.052	8

analytical, whereas the second one is provided by BI-RME.

Figure 4 depicts the relative error in the computation of coupling integrals between two sets of modes using the rectangular-based implementation. In all cases the exact value for the coupling integrals is taken as the convergent value provided by the circular-based implementation. In Fig. 4b the coupling integral between the first mode of the cross-shaped waveguide and the first mode of the circular waveguide is shown, for different values of N_r. In Fig. 4c, the coupling coefficient between a high-order mode (35th) of the cross-shaped waveguide and a high-order mode (257th) of the circular waveguide is depicted. The criteria for choosing these particular combinations of modes has been that a significant coupling ($I_{\bigcirc}^{\triangle} > 0.1$) between them should exist.

The main conclusion that can be drawn from both graphs is that the rectangular-based implementation, even though it provides accurate results when low-order modes are involved, lacks some accuracy when dealing with higher order ones. The reason for this loss in accuracy is that high-order modes have complex field patterns, which are represented in a less accurately way by a series of rectangular waveguide modes. Meanwhile, the circular-based implementation does not need to represent these arbitrary modes by any series, but instead defines them by the modal current density computed by the BI-RME method. Therefore, the computation of the coupling coefficients of these high-order modes has the same accuracy level as the corresponding modal chart computation.

Considering high-order modes is important when complex structures are studied, specially when the arbitrary waveguide is used as an iris. In such cases, the circular-based implementation offers an important advantage over the rectangular-based algorithm when some of the interconnections involve arbitrary and circular waveguides.

Finally, it is worth noting the oscillatory behaviour of the coupling integrals with the different number of

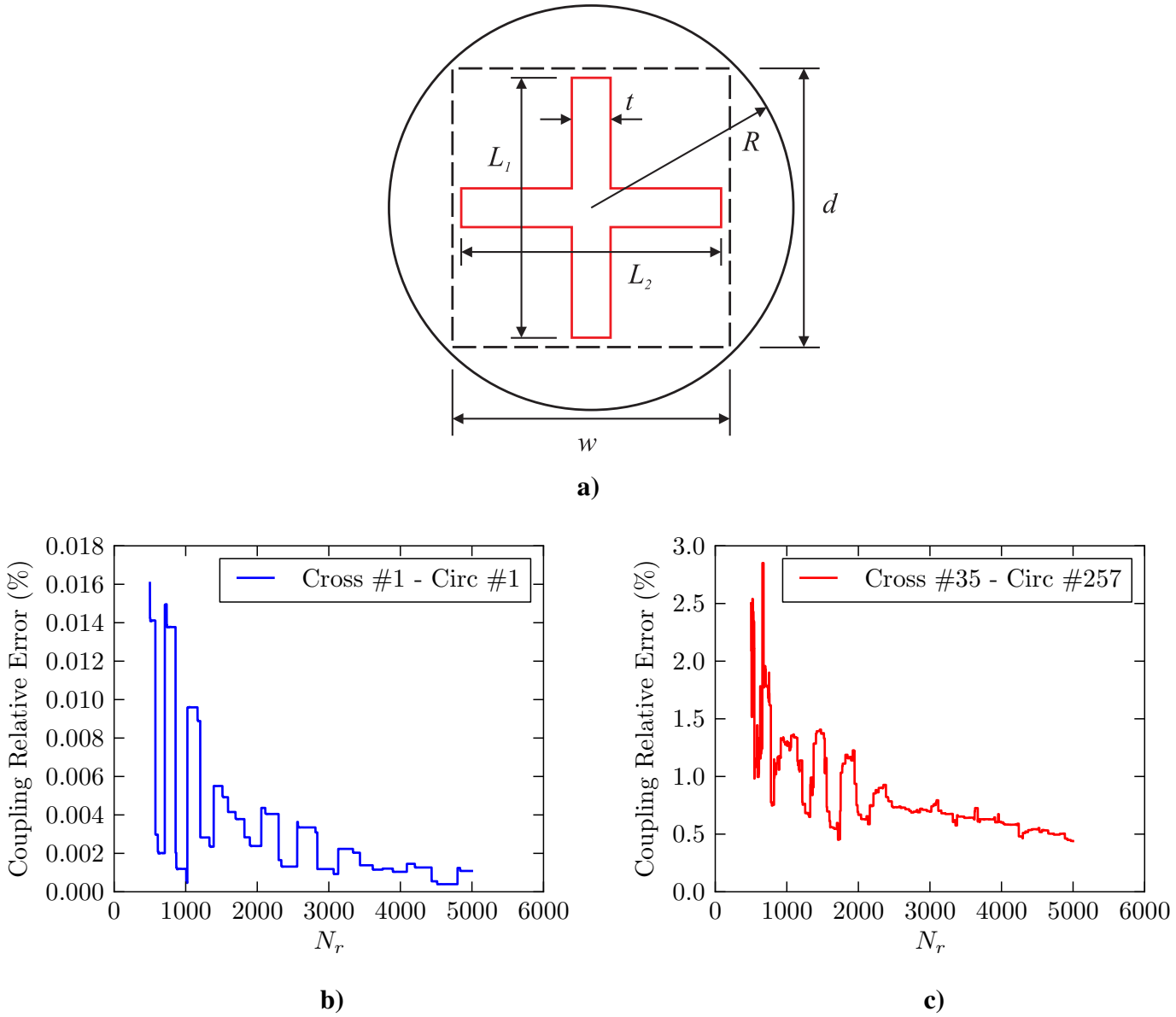

Fig. 4. **a)**: Cross-shaped iris of dimensions $L_1 = 17.3$ mm, $L_2 = 15.3$ mm, $t = 2$ mm connected to a circular waveguide of radius $R = 12$ mm. Dashed lines represent the contour of dimensions $w = 15.4$ mm, $d = 17.4$ mm used for the application of the rectangular-based algorithm.

b): Relative error in the computation of coupling integrals between the first cross-shaped mode and the first circular waveguide mode using the rectangular-based implementation. The exact value to compute the error is taken as the one provided by the circular-based implementation.

c): Relative error in the computation of coupling integrals between the 35th cross-shaped mode and the 257th circular waveguide mode using the rectangular-based implementation.

rectangular modes, which may produce inaccurate results if a proper convergence study is not previously carried out.

D. Circular Waveguide Polariser

After comparing the performance of the circular-based and rectangular-based implementations of the BI-RME method with certain waveguide structures, the analysis of complete components based on circular waveguides has been considered. As a first example, a circular waveguide polariser has been analysed both using the circular-based and the rectangular-based implementations. This component is based on a series of multi-ridged circular waveguides, as can be seen in Fig. 5a, hence the response is expected to be computed more accurately with the circular-based implementation.

In Fig. 5b, the response obtained by both implementations is shown and compared with the measured response of a prototype included in [18]. For the vertical polarization, where the magnitude of the response has higher values, both implementations provide accurate results, coincident with the measurements. However, the circular-based implementation obtains more accurate results than the rectangular-based code for the horizontal polarization, judging by the measured response.

Once the accuracy of both implementations is compared, we proceed to compare its efficiency. In order to obtain the depicted convergent response, 600 resonant modes of the circular contour and 4000 of the rectangular contour have been used. This important reduction in the number of resonant modes, combined with the reduction from 404 to 48 in the number of segments considered by the BI-RME method, justifies the notable difference in computation time: the circular-based implementation takes 40 s to properly solve the structure for 100 frequency points while the rectangular-based algorithm takes 169 s to obtain a response that is less accurate.

E. Analysis of a Dual-Mode Filter with Elliptical Irises and Tuning Elements

Another example that has been considered is the full-wave analysis of the dual-mode filter designed in [19]. Its geometry, which can be seen in Fig. 6, is composed of two sections of circular waveguide perturbed by three triangular metallic insertions, which provide intra-cavity couplings and frequency adjustment, and connected through elliptic irises which provide inter-cavity and input/output couplings.

The analysis of this structure with the circular-based implementation has been compared in Fig. 7 with the simulated responses provided by both the rectangular-based algorithm and measurements of the manufactured prototype presented in [19]. The results show that the circular-based algorithm is more accurate for this particular structure, heavily based on circular waveguide technology. Measurements are highly coincident with the response obtained by the circular-based algorithm, which properly simulates the measured bandwidth. The slight disagreements between the measured and simulated responses from [19] (i.e. the rectangular-based algorithm) can be explained by the high sensitivity level of this device, meaning that any error in the computation of the modal charts and coupling coefficients has an important effect in the accuracy of the overall response.

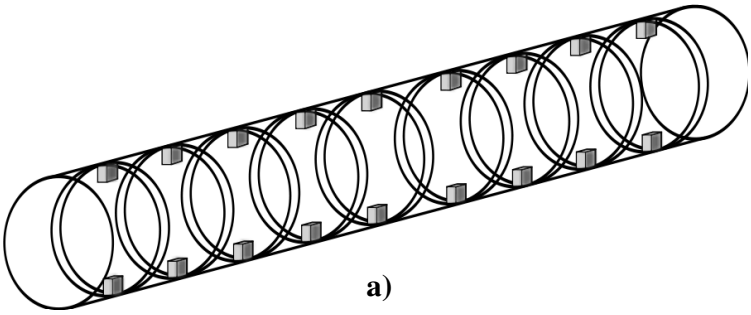

a)

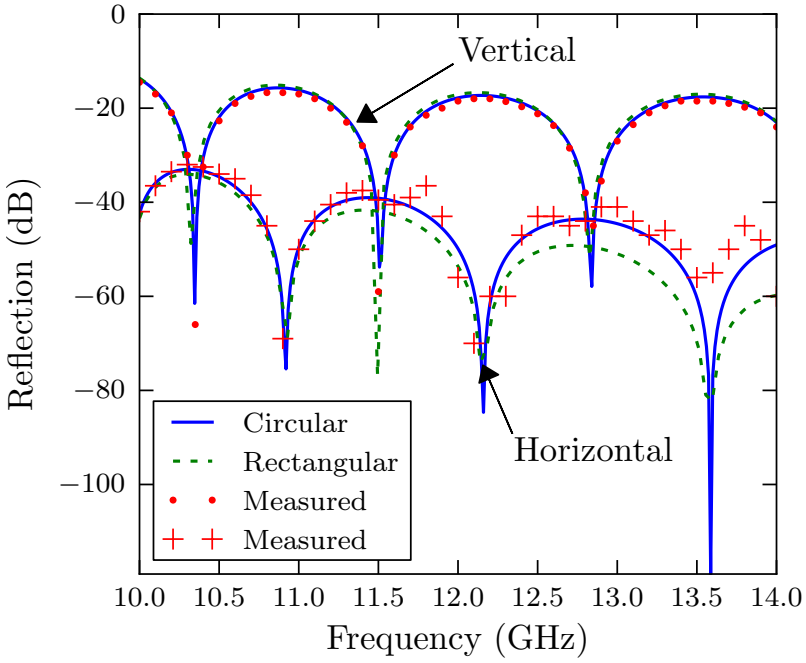

b)

Fig. 5. **a)**: Magnitude of the reflection coefficient (S_{11}) of the circular waveguide polariser presented in [18] for vertical and horizontal polarizations. Simulated results with the circular-based (solid lines) and rectangular-based implementations (dashed lines) are compared with measured results (dots and crosses) extracted from the aforementioned article.
b): Magnitude of the reflection coefficient (S_{11}) of the circular waveguide polariser presented in [18] for vertical and horizontal polarizations. Simulated results with the circular-based (solid lines) and rectangular-based implementations (dashed lines) are compared with measured results (dots and crosses) extracted from the aforementioned article.

As far as the computational efficiency of the presented algorithm is concerned, it is clear that the performance of the circular-based implementation is unparalleled by the rectangular-based one. To achieve the convergent results depicted in Fig. 7, the circular-based implementation took just 60 s to compute 100 frequency points while the rectangular-based one took twice as much time, a total of 140 s. Along with the increase of resonant modes and number of segments that the rectangular-based code required, an important increase in the number of accessible modes, basis functions and kernel terms was also necessary to solve the complete structure.

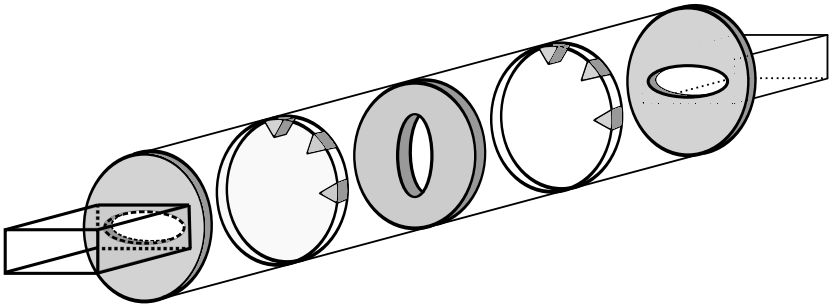

Fig. 6. Physical structure of the dual-mode filter consisting of triangular insets and elliptical irises. The insets, located at 0° (horizontal), 45° and 90° (vertical), have the following dimensions: $4.1\ \text{mm} \times 1.88\ \text{mm}$, $3.61\ \text{mm} \times 1.88\ \text{mm}$, $3.61\ \text{mm} \times 1.88\ \text{mm}$, respectively, and $2\ \text{mm}$ thick. The dimensions of the input and output elliptical irises are: major axis $12.78\ \text{mm}$, minor axis $4\ \text{mm}$ and $1.66\ \text{mm}$ thick. The inter-cavity elliptical iris has a major axis of $8.7\ \text{mm}$, minor axis of $4\ \text{mm}$ and $1.79\ \text{mm}$ thick. The circular waveguides, of radius $12\ \text{mm}$, are $7.34\ \text{mm}$ long each.

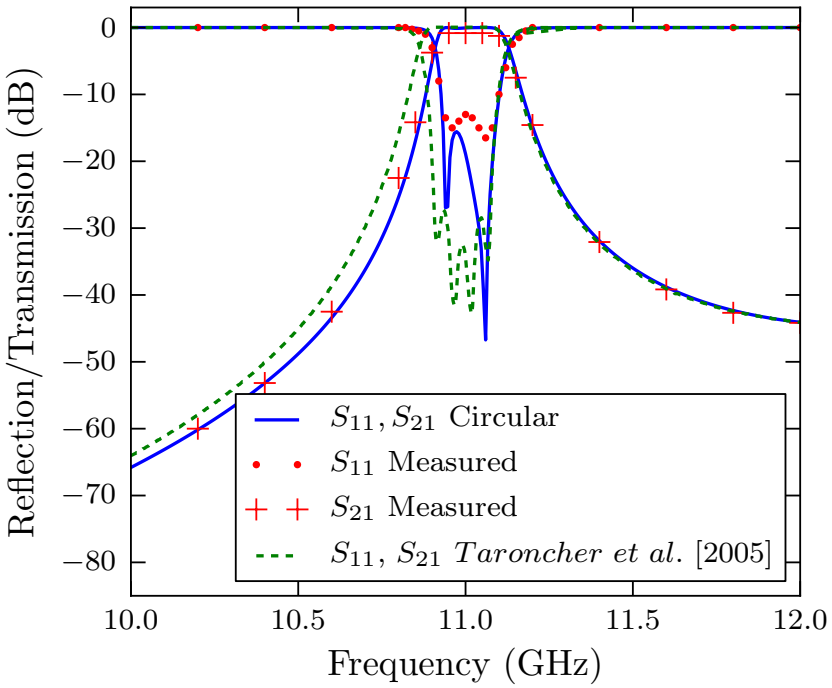

Fig. 7. Magnitude of the reflection (S_{11}) and transmission (S_{21}) coefficients of the dual-mode filter consisting of triangular insets and elliptical irises. Solid lines denote the authors' results, dashed lines denote the simulated response presented in [19] (i.e. rectangular-based implementation), and the circles and crosses correspond to the prototype measured data.

F. Design of a Dual-Mode Filter with Cross-Shaped Irises and Tuning Elements

The last example deals with the design of a complex passive device in circular waveguide technology. The structure under consideration is the four-pole dual-mode filter depicted in Fig. 8, along with its dimensions. It is based on two circular waveguides coupled through a cross-shaped iris and includes two sets of tuning elements, a classical structure widely used in satellite communications [20]. After designing the device, a prototype of this dual-mode filter has been manufactured with real rectangular insets to validate the analysis tool presented in this article.

Figure 9 depicts the response of this manufactured prototype compared with the simulated response obtained with the circular-based and the rectangular-based BI-RME implementations. The response simulated with the circular-based code is almost identical to the measured one, confirming the accuracy of this tool when dealing with these complex devices. Regarding the rectangular-based response, a small frequency shift of approximately 7 MHz is observed. Additionally, the out-of-band response of the filter up to 20 GHz is successfully compared with measurements.

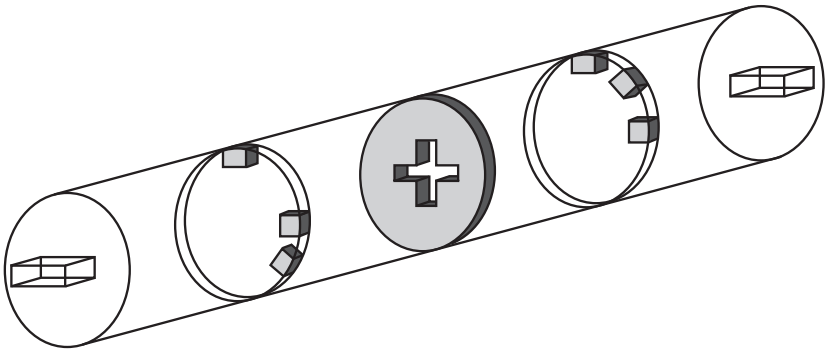

Fig. 8. Physical structure of the designed dual-mode filter in a circular waveguide of radius 13.3 mm. The first cavity is 54.4366 mm long, and the second is 54.4436 mm long. The dimensions of the coupling structures are as follows: Input and output rectangular irises (10.6441 mm $\times$ 2 mm) of length 1 mm. First triple-inset coupling section (thickness 2 mm) has its insets (2 mm wide) located at angles 0° (horizontal), 90° (vertical) and 315°. The penetration depths of these insets are 2.8956 mm, 1 mm and 1.9345 mm, respectively. Cross iris of thickness 1 mm with vertical and horizontal arms of 7.688 mm and 4.407 mm, respectively, and 1 mm wide. Second triple-inset coupling section of thickness 2 mm with 2 mm wide insets located at angles 0°, 45° and 90° of depths 2.9023 mm, 2.0364 mm and 1 mm, respectively.

As far as the computational efficiency of the analysis is concerned, the circular-based algorithm takes advantage of a more accurate characterization of the tuning sections, as well as a faster characterization of the different planar junctions to achieve convergent results in a shorter amount of time. While the rectangular-based implementation takes 100 s to compute 100 frequency points, the circular-based implementation takes just 43 s, a considerable reduction of the computation time just by using the appropriate resonant contour.

IV. Conclusions

In this paper, an important enhancement of previous implementations of the BI-RME method has been presented. This new implementation is intended to analyse passive devices based on circular and arbitrarily-shaped waveguides in a more accurate and efficient way. It combines a circular contour as resonant structure with the inclusion of straight, circular and elliptical arcs for defining the perturbed geometry. Compared with previous implementations of the same method based on rectangular waveguides, this implementation takes advantage of a lower number of resonant modes for the accurate modelling of the arbitrary sections, as well as the efficient computation of coupling coefficients between circular and arbitrary-shaped waveguides. Therefore, the analysis of devices based on circular

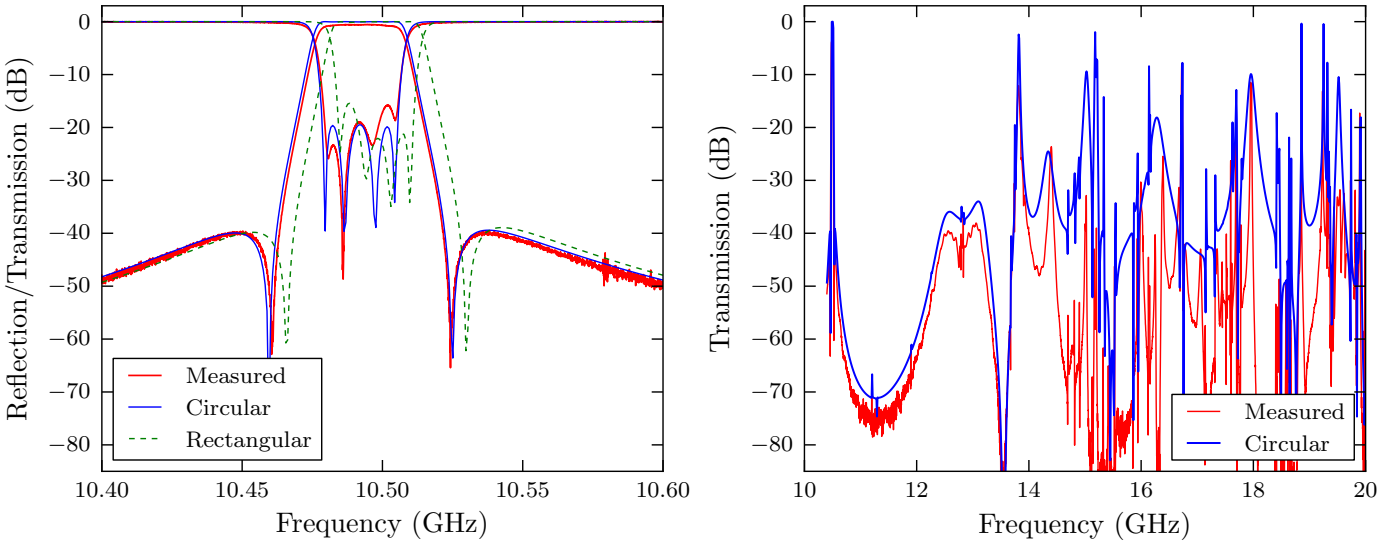

Fig. 9. In-band and out-of-band response of the designed dual-mode filter. Measurements of a manufactured prototype are compared with the simulation of the circular-based implementation.

and arbitrary waveguides is highly improved by the use of the proposed implementation, as it has been shown through some examples. The accuracy of this new implementation has also been successfully verified using several examples of practical interest, comparing the simulated responses with data taken from technical literature and experimental measurements. Furthermore, a dual-mode filter prototype has been designed and manufactured for this purpose. In all the examples, the performance of the new implementation has been optimum, especially when compared with the previous rectangular-based implementation.

V. Acknowledgments

This work was supported by Ministerio de Ciencia e Innovación, Spanish Government, under Research Project TEC2010-21520-C04-01.

References

[1] Cameron RJ, Kudsia CM, Mansour RR. Microwave Filters for Communication Systems. Hoboken, NJ: John Wiley & Sons; 2007.

[2] Boria VE, Gimeno B. Waveguide Filters for Satellites. IEEE Microwave Magazine. 2007 October;8(5):60–70.

[3] Schroeder WL, Guglielmi M. A contour-based approach to the multimode network representation of waveguide transitions. IEEE Trans Microwave Theory Tech. 1998 April;46(4):411–419.

[4] Omar AS, Schunemann KF. Application of the generalized spectral-domain technique to the analysis of rectangular waveguides with rectangular and circular metal inserts. IEEE Trans Microwave Theory Tech. 1991 June;39(6):944–952.

[5] Silvester PP, Pelosi G. Finite Elements for Wave Electromagnetics. New York: IEEE Press; 1994.

[6] Taflove A. Computational Electromagnetics: The Finite-Difference Time-Domain Method. Norwood, MA: Artech House; 1995.

[7] Montejo-Garai JR, Zapata J. Full-wave design and realization of multicoupled dual-mode circular waveguide filters. IEEE Trans Microwave Theory Tech. 1995 June;43(6):1290–129.

[8] MacPhie RH, Wu KL. A full-wave modal analysis of arbitrarily shaped waveguide discontinuities using the finite plane-wave series expansion. IEEE Trans Microwave Theory Tech. 1999 February;47(2):232–237.

[9] Arndt F, Brandt J, Catina V, Ritter J, Rullhusen I, Dauelsberg J, et al. Fast CAD and optimization of waveguide components and aperture antennas by hybrid MM/FE/MoM/FD methods State-of-the-art and recent advances. IEEE Trans Microwave Theory Tech. 2004 January;52(1):292–305.

[10] Conciauro G, Guglielmi M, Sorrentino R. Advanced Modal Analysis - CAD Techniques for Waveguide Components and Filters. Chichester, England: John Wiley & Sons; 2000.

[11] Conciauro G, Bressan M, Zuffada C. Waveguide modes via an integral equation leading to a linear matrix eigenvalue problem. IEEE Trans Microwave Theory Tech. 1984 November;32(11):1495–1504.

[12] Arcioni P. Fast evaluation of modal coupling coefficients of waveguide step discontinuities. IEEE Microwave Guided Wave Lett. 1996 June;6(6):232–234.

[13] Cogollos S, Marini S, Boria VE, Soto P, Vidal A, Esteban H, et al. Efficient Modal Analysis of Arbitrarily Shaped Waveguides Composed of Linear, Circular, and Elliptical Arcs Using the BI-RME Method. IEEE Trans Microwave Theory Tech. 2003 December;51(12):2378–2390.

[14] FEST3D 6 6 0; 2011. Aurora Software and Testing, S.L. on behalf of ESA/ESTEC, Valencia, Spain, www.fest3d.com.

[15] Zhang SJ, Shen YC. Eigenmode sequence for an elliptical waveguide with arbitrary ellipticity. IEEE Trans Microwave Theory Tech. 1995 January;43(1):227–230.

[16] Balaji U, Vahldieck R. Radial mode matching analysis of ridged circular waveguides. Microwave Theory and Techniques, IEEE Transactions on. 1996 July;44(7):1183 –1186.

[17] Dillon BM, Gibson AAP. Triple-ridged circular waveguides. J of Electronzag Waves Applicat. 1995 January;9(1-2):145–156.

[18] Montejo-Garai JR, Zapata J. Full-wave design of dual-band double-septum circular waveguide polarizers. Microwave Opt Technol Lett. 1999 January;20(2):99–103.

[19] Taroncher M, Vidal A, Boria VE, Marini S, Cogollos S, Gil J, et al. CAD of complex passive devices composed of arbitrarily shaped waveguides using Nyström and BI-RME methods. IEEE Trans Microwave Theory Tech. 2005 June;53(6):2153–2163.

[20] Kudsia C, Cameron R, Tang WC. Innovations in Microwave Filters and Multiplexing Networks for Communications Satellite Systems. IEEE Trans Microwave Theory Tech. 1992 June;40(6):1133–1149.